Journal of Polymer Research (2022) 29: 328
https://doi.org/10.1007/s10965-022-03153-9

ORIGINAL PAPER

Green synthesis of covalent hybrid hydrogels containing PEG/PLA-based thermoreversible networks

Sirine Mhiri[1,2] · Majdi Abid[3] · Souhir Abid[3] · Frederic Prochazka[1] · Caroline Pillon[1] · Nathalie Mignard[1]

Received: 1 March 2022 / Accepted: 19 June 2022 / Published online: 14 July 2022

Abstract

A series of thermosensitive polyethylene glycol (PEG)-polylactic-acid (PLA)-based hydrogels were synthesized, through the Diels–Alder reaction, with tunable hydrophilicity and hydrophobicity. Polyethylene glycol (PEG) was end-functionalized with furan groups using a synthetic furanic diol prepared by thiol-ene reaction. Functional maleimide PLA was prepared from PLA-diol, glycerol, 4,4′-methylenebis(cyclohexyl isocyanate) (H_{12}MDI) and N-hydroxymethylmaleimide (HMM), by the isocyanate-alcohol condensation reaction. FTIR, ^{1}H NMR, DSC, and SEC studies of the prepared precursors were carried out. Then, an organic solvent-free environmentally friendly synthesis was used to obtain the cross-linked Diels–Alder adducts, by changing the feeding ratio of PEG/PLA. The rheological studies proved the success of using Diels–Alder reaction, confirming the formation of cross-linked networks and its thermal dependence. After proceeding with their characterizations, the obtained adducts were brought into contact with the water leading to the formation of hydrogels. Swelling measurements revealed that the chemical composition influenced the swelling and the water diffusion mechanism of hydrogels. Finally, we found that hydrolytic degradation was governed by ester bond hydrolysis that could be controlled by adjusting the composition ratio of PEG to PLA.

Keywords Diels–Alder · Amphiphilic hydrogel · Reactive extrusion · Thermoreversibility

Introduction

Polymeric hydrogels are cross-linked materials composed of hydrophilic macromolecules whose particularity is to retain a high amount of water [1]. Thanks to their soft consistency, the wide variety of their synthesis methods and their physical and tunable characteristics, biocompatible hydrogels have emerged as one of the most desirable cross-linked biomaterials used for many applications in regenerative medicine, biotechnology, pharmaceutical, cosmetics, or plastics sectors [2, 3].

Hydrogels can be synthesized from natural, synthetic, or hybrid polymers [4]. As natural polymers, a variety of polysaccharides like chitosan, dextran, and alginate have generated a great interest owing to their good biological properties, as well as excellent gel-forming properties [5]. Synthetic polymers, such as poly(acrylic acid), and its derivatives, poly(ethylene oxide) and polypeptides, exhibit good mechanical strength [6]. Among the hydrophilic synthetic polymers used in the preparation of hydrogels, poly(ethylene glycol) (PEG) is one of the most encountered. Being a non-immunogenic and non-cytotoxic hydrophilic polymer, PEG is approved by the FDA and has found widespread application in the design of biomaterials for the controlled release of active molecules and tissue repair systems [7–9]. Despite these obvious advantages, PEG is not biodegradable and this restricts its use in tissue engineering. Currently, there is an increased interest in biodegradable hydrogels for regenerative medicine field used as scaffolds, delivery systems, as they do not require any surgical removal process [10]. In this respect, combining PEG with a biodegradable polymer could represent a potential solution for adjusting the biodegradability

✉ Nathalie Mignard
nathalie.mignard@univ-st-etienne.fr

1 UMR 5223, Univ Lyon, CNRS, Université Claude Bernard Lyon1, INSA Lyon, Université Jean Monnet, Ingénierie des Matériaux Polymères, 42000 Saint Etienne Cedex, France

2 Laboratoire de Chimie Appliquée HCGP, Faculté Des Sciences de Sfax, Université de Sfax, 3000 Sfax, Tunisie

3 Chemistry Department, College of Science and Arts, Jouf University, Al Qurayyat, Al Jouf, KSA, Saudi Arabia

of PEG-based hydrogels. Poly(lactic acid) (PLA) is one of the most used biodegradable polymer for biomedical application, because of its suitable mechanical and biological properties [11, 12]. It has been extensively studied in the literature, as the hydrophobic building blocks of amphiphilic hydrogels, to control the water uptake of these hydrogels while allowing predictable control of degradation's rates [13].

Hydrogels can be chemically or physically cross-linked. Chemically cross-linked hydrogels endow good mechanical and structural stability generally better than those of physically cross-linked hydrogels [14]. However, the use of reagents, suitable catalysts, or photoinitiators during chemical cross-linking affects inevitably the biocompatibility of the final material [15].

The Diels–Alder reaction (DA) represents in this context an ideal and selective way to overcome the disadvantages detected in most chemical cross-linking process. Indeed, it allows the development of covalent hydrogels under mild conditions without any additive and without producing side reactions [16]. Diels–Alder chemistry involves the reaction between a diene and a dienophile, typically furan and maleimide functional precursors [17, 18]. The interest in the exploitation of furan compounds is due to their renewable nature and their pronounced diene character, which favors the reaction in terms of yield and kinetics [19]. The maleimide group is the most used dienophile function in the DA reaction thanks to its reactivity enhanced by electron attractive groups [20]. DA reaction is a thermosensitive equilibrium, which is displaced towards reactants at high temperature by the rDA (reverse Diels Alder) reaction. This property can be used for the synthesis of dry networks for hydrogel creation in a green solvent-free process [21].

This work focuses on the development of hybrid hydrogels containing hydrophilic/hydrophobic blocks formulated from PEG and PLA through the Diels–Alder reaction. PEG and PLA were functionalized with furyl and maleimide groups, respectively. The obtained precursors, furan-terminated PEG (PEG-F) and trimaleimide-terminated PLA (PLA-Tri M), were then used for hydrogels preparation. First, Diels–Alder adducts were synthesized via the reactive extrusion process by modulating the balance of PEG-F and PLA-Tri M. The choice of this method offers the advantage of not using solvent and ensuring continuous production. Once obtained, their immersion in water leads to the formation of hydrogels. The thermoreversibility of Diels–Alder adducts was assessed by rheology experiments. The microstructure, swelling properties, diffusional behavior, thermal reversibility, and hydrolytic degradation of hydrogels were studied, and properties were then discussed according to the hydrophilic/hydrophobic balance.

Experimental

Materials

Hydroxytelechelic PEG with a number average molecular weight $\overline{M_n} = 1550$ g.mol^{-1} was provided by Fluka. Prior to use, L-lactide (PURAC, PURASORB) was dried under vacuum at 50 °C for 24 h. Glycerol (99%), tin 2-ethylhexanoate (Sn $(Oct)_2$, 95%), dibutyltin dilaurate (DBTDL, 95%), 3-allyloxy-1,2-propanediol (AP, 99%), 2-furanmethanethiol (FMT, 97%), 2,2′-azobis (2-methylpropionitrile) (AIBN, 98%), 4,4′-methylene bis (cyclohexyl isocyanate) (H_{12}MDI, 90%), 1,4-butanediol (BD, 99%), N,N-dimethylformamide (DMF, anhydrous, 99.8%), acetone (99.5%), and tetrahydrofuran (THF, anhydrous, 99.9%) were all purchased from Sigma Aldrich. Furfuryl alcohol (FAL, 98%) was supplied by Acros Organics. N-hydroxymethylmaleimide (HMM) was prepared according to the method described by Tawney et al. [22] (synthesis and characterization (Figs. S1, S2, and S3) are given in supplementary data). DMF, THF, and glycerol were dehydrated by 4 Å molecular sieves for 48 h before use, and the other reactants were used without further purification.

Synthesis of 3-(3-furfurylmercaptan propoxy) propane-1,2-diol by thiol-ene reaction (FD)

3-(3-furfurylmercaptan propoxy) propane-1,2-diol (FD) was synthesized by thiol-ene reaction between 3-allyloxy-1,2-propanediol (AP) and 2-furanmethanethiol (FMT). Thirty grams of AP (0.227 mol) and 25.91 g of FMT (0.227 mol) were introduced in a round bottom flask, at room temperature in THF. 0.164 g of AIBN (0.001 mol), dissolved in THF, was then added and the homogenized mixture was refluxed at 70 °C. The reaction was followed by FTIR in order to verify the evolution of the double bond as a function of time. Complete conversion was obtained after 24 h of reaction. The solvent was then removed by evaporation under reduced pressure. The organic phase was washed with water to remove the residual AP and dried over magnesium sulfate.

Synthesis of furan-functionalized polyethylene glycol (PEG-F)

Three samples of furan-functionalized PEG with different PEG diol content and the same furan functionality were synthesized. In PEG-Fi, i is the percentage of the PEG-F used for the synthesis of adducts.

Table 1 includes the stoichiometry ratio used for the different syntheses.

Table 1 Molar ratios of furan-functionalized PEG

Samples	PEG-diol	FD	H_{12}MDI	FAL
PEG-F_{40}	1	1	3	2
PEG-F_{60}	2	1	4	2
PEG-F_{90}	6	1	8	2

The synthesis of PEG-F_{60} with a furan-functionality of 3 is given as an example.

In a 100-mL flask equipped with magnetic stirring, 20 g of PEG-diol (0.0129 mol), 1.6 g of FD (0.00645 mol), and 6.77 g of H_{12}MDI (0.0258 mol) were introduced. The reaction mixture was stirred at 50 °C in 60 mL of acetone under nitrogen atmosphere in the presence of 0.14 g of DBTDL as catalyst. FTIR was used to follow the evolution of the isocyanate absorption band as a function of time. Once the band of the isocyanate remained invariable, 1.26 g (0.0129 mol) of FAL was added. At the end of the reaction, the solvent was evaporated in a vacuum oven at 50 °C for 12 h.

Hydroxyl telechelic polylactic acid (PLA-diol)

PLA hydroxyl-telechelic oligomer was obtained by ring opening polymerization of L-lactide monomer catalyzed by tin (II) 2-ethylhexanoate following a previously reported procedure [23].

A typical synthesis procedure is shown below: 80 g of L-lactide (0.55 mol) and 12.35 g of 1,4-butanediol (0.14 mol) were introduced into a 150-mL three-necked flask under nitrogen atmosphere. The reaction mixture was conducted at 110 °C until homogenization. Then, 2.25 g of the catalyst ($Sn(Oct)_2$) (0.005 mol) was added dropwise. The system was maintained under mechanical stirring for 6 h. The resulting PLA-diol was obtained as a white waxy solid.

Maleimide-modified PLA (PLA-Tri M)

PLA-diol was end-functionalized with maleimide through the reaction of its hydroxyl groups with diisocyanate and multi-alcohol to obtain tailored structure of PLA-Tri M with a functionality of 3.

A typical synthesis procedure is shown below: in a 150-mL three-necked flask equipped with magnetic stirring, 20 g of PLA-diol (0.0277 mol), 0.85 g of glycerol (0.0092 mol), and 16 g of H_{12}MDI (0.0611 mol) were firstly dissolved in anhydrous DMF. The reaction mixture was stirred at 80 °C under nitrogen atmosphere. Subsequently, 0.37 g of DBTDL (0.0006 mol) acting as a catalyst was injected after the homogenization of the system. The reaction was monitored by FTIR until the isocyanate absorption band at 2263 cm^{-1} remained stable. Then, 4.93 g of HMM (0.0253 mol) were introduced and the reaction was maintained until the total consumption of the isocyanate group. At the end of the reaction, the resulting reaction product was precipitated in diethyl ether and then dried under vacuum at 50 °C for 24 h.

Table 2 Composition of Diels–Alder adducts

Designation	Composition	PEG-F_i/PLA-Tri M %wt/%wt
$PE_{40}PL_{60}$	PEG-F_{40}/PLA-Tri M	40/60
$PE_{60}PL_{40}$	PEG-F_{60}/PLA-Tri M	60/40
$PE_{90}PL_{10}$	PEG-F_{90}/PLA-Tri M	90/10

Hydrogel preparation by DA reaction

Various formulations of Diels–Alder hydrogels were prepared by modulating the ratio of hydrophilic/hydrophobic prepolymers. First, dry adducts were synthesized via reactive extrusion, by mixing PLA-Tri M and PEG-F, respecting the equifunctionality of furan and maleimide functions and with proportions allowing the obtaining of similar nodes concentration.

The appropriate weights of the two precursors were introduced in the extruder and mixed in different ratios at 90 °C (Table 2). After slow cooling to room temperature, the cross-linking of the mixture was carried out via the Diels–Alder reaction. The formation of hydrogels was achieved by the incubation of adducts in water.

Swelling properties of hydrogels

Swelling behavior of hydrogels was studied by a general gravimetric method by measuring the weight gain over a period of time until equilibrium was reached. DA adducts were incubated in deionized water at 25 °C and 37 °C. At regular time intervals, the swollen gels were removed and the excess water remaining on the surface was carefully dried with filter paper. The swelling rate was calculated using the following equation:

$$SR(\%) = \frac{(Ws - Wd)}{Wd} \times 100 \quad (1)$$

where W_d is the initial weight of DA adducts and W_s is the weight of swollen hydrogels. The equilibrium swelling was considered to be reached when the weight of the hydrogels no longer increased with time.

Hydrolytic degradation

The hydrolytic degradation tests were carried out on the obtained hydrogels in three different media with different pH values. Previously weighted hydrogels were immersed in closed vials containing one of the following buffer solution: acidic aqueous solution (pH = 4.35) phosphate buffer (pH = 7.4) and basic solution (pH = 9.5). The vials were maintained under inert conditions at 37 °C for 10 weeks. The samples were taken once a week, washed with distilled water, dried under vacuum, and then weighed using a precision balance to determine the remaining masses.

The percentage of weight loss (w_l) was calculated according to the following equation:

$$w_1(\%) = \frac{m_o - m_t}{m_o} \times 100 \quad (2)$$

where m_t stands for the weight of dried samples and m_0 is the initial weight.

Analytical techniques

The samples were characterized by Fourier transformed infrared spectroscopy (FTIR) using a Nexus-type Nicolet spectrometer in attenuated total reflectance (ATR) mode. Spectra were collected for all the samples at room temperature in the range of 700–3700 cm^{-1} with a spectral resolution of 4 cm^{-1} for a total of 64 scans.

Proton nuclear magnetic resonance (^{1}H-NMR) spectra were acquired on a Brüker Avance Fourier transform apparatus having a nominal frequency of 400 MHz. Solvent used was deuterated chloroform (δ = 7.26 ppm) or deuterated DMSO (δ = 2.5 ppm) at 80 °C and TMS (tetramethylsilane) was used as reference.

Number average molecular weight ($\overline{M_n}$), weight average molecular weight ($\overline{M_w}$), and polydispersity index (D_m) of the PEG-F and PLA-Tri M precursors were estimated by size exclusion chromatography (SEC) system equipped with a 515 HPLC pump, a 717 plus autosampler, and a 2414 refractive index detector. Additionally, a Wyatt ViscoStar viscometer and a WYATT miniDAWN TREOS multiangle light scattering detector were used. The flow rate of tetrahydrofuran (THF, Biosolve, GPC grade) in the mobile phase was 1 mL/min. The dissolution of each sample was first performed at room temperature for 15 min.

Differential scanning calorimetry (DSC) experiments were performed using a TA Q10 instrument under nitrogen atmosphere (50 mL/min). The method consists of imposing a rise in temperature from − 80 °C up to 200 °C at a heating and cooling rates of 10 °C/min. The glass transition temperatures (Tg) and the melting temperatures (Tm) were taken respectively at the inflection point of the curve by means of the melting endotherm during the second pass.

Thermogravimetric analyses (TGA) were carried out on a METTLER TOLEDO TGA/DSC thermogravimetric analyzer. The samples were placed in aluminum crucibles and ramped at 30 to 600 °C at a heating rate of 10 °C/min under inert atmosphere. The thermal degradation temperatures (Td) recorded correspond to a 5% weight loss of the samples.

The rheological properties of the hydrogels and adducts were evaluated using an Advanced Rheometric Expansion System (ARES-G2) rheometer operating with parallel plate geometry (25 mm diameter). The dynamic rheological analysis of DA adducts was carried out by first performing a strain sweep of 0.1 to 100% at 1 Hz to identify the linear viscoelastic range of the samples. Then, a destruction of networks was ensured, by keeping the samples between the two plates of the rheometer at 120 °C for 5 min, by adopting the same procedure carried out in our previous publication [24]. Maturation and frequency sweep tests of the adducts were performed at 80 °C to ensure the cross-linking Diels–Alder equilibrium and measure the elastic and shear loss moduli, respectively. Temperature sweep experiments were realized at 1 rad s^{-1} frequency and 5 °C/min and 1 °C/min, respectively, heating and cooling rate constant. Frequency sweep measurements for hydrogels were performed at 25 °C and 37 °C, at a fixed strain previously assessed by stress sweep experiments.

A micro-compounder HAAKE™ MiniLab II from Thermo SCIENTIFIC France, equipped with two conical screws (5/14 mm diameter), a pneumatic bypass and a recirculation channel, was used in co-rotating mode and operating at 50 rpm, monitored by MiniLab software. Seven grams of PLA-Tri M and PEG-F was first premixed and then introduced into the mixer at 90 °C. After about 10 min, where stable torque is reached, the mixtures were left for about 5 min and then extruded as a flat rod about 1.5 mm thick and 5 mm wide. This was then cooled to room temperature.

Results and discussion

Synthesis and characterization of hydrogel precursors

Synthesis of 3-(3-furfurylmercaptan propoxy) propane-1,2-diol (FD)

An efficient approach for the synthesis of a furan compound with dihydroxyl group was developed (Scheme 1). The significant interest of this method is its simplicity and its effectiveness to substitute the commercial furanic products, which are still too expensive. The radical addition of the FMT to the AP was carried out by the thiol-ene reaction between the allyl group of AP and thiol group

Scheme 1 Synthesis of 3-(3-furfurylmercaptan propoxy) propane-1,2-diol (FD) by thiol-ene reaction

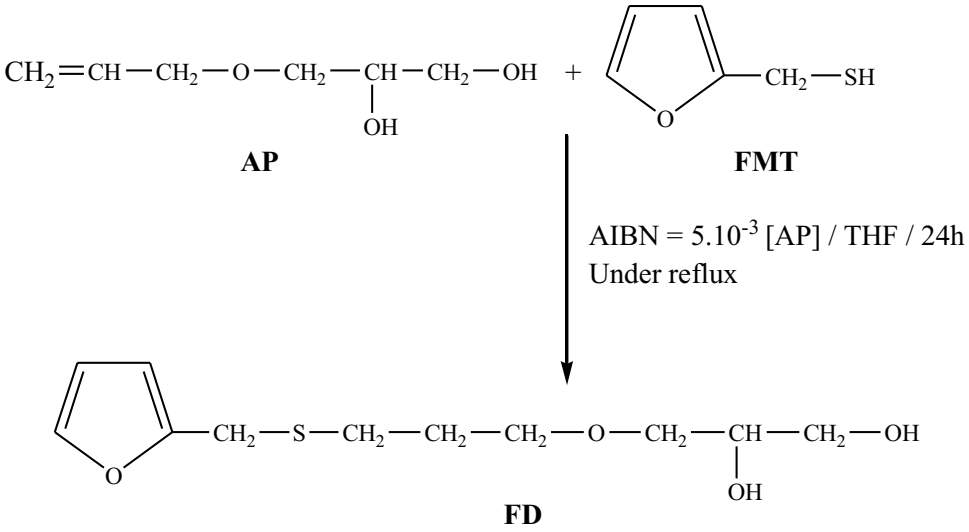

of FMT. The 3-(3-furfurylmercaptan propoxy) propane-1,2-diol was obtained according to the following reaction scheme:

The success of this reaction was confirmed by FTIR spectroscopy (Fig. S4 in SI) and expected chemical structure of FD was confirmed by ^{1}H-NMR spectrum (Fig. S5 in SI).

Synthesis of furan-functionalized polyethylene glycol (PEG-F)

In order to be able to modify the hydrophilic/hydrophobic balance in the networks' structure with PEG-F and PLA-Tri M polymers, while respecting the equifunctionality of furan and maleimide groups, various PEG-F precursors were synthesized. The functionality of furan was maintained for all samples; only the concentration of furan functions by weight was varied by modifying the quantities of PEG-diol and H_{12}MDI.

FD previously synthesized by thiol-ene reaction was subsequently used to obtain furan-functionalized PEG according to the reaction scheme presented below for the synthesis of (PEG-F_{60}) (Scheme 2). This synthesis was carried out via two-step reactions. During the first step, PEG-diol was reacted with the isocyanate and the 3-(3-furfurylmercaptan

Scheme 2 Synthesis of PEG-F_{60}

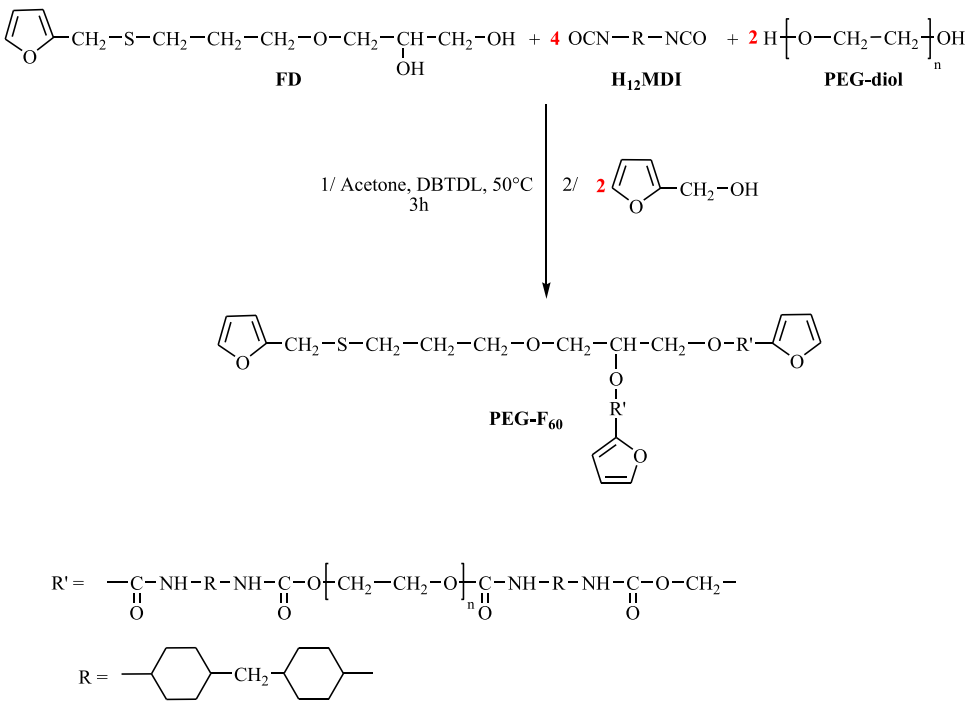

propoxy) propane-1,2-diol to gain intermediate bearing free–NCO groups. In the second part, FAL was added to the reaction mixture to give the desired compound PEG-F_{60}.

The progress of the alcohol-isocyanate reaction was tracked by FTIR, as shown in Fig. 1. In the first step of reaction, the isocyanate carbonyl absorption band at 2263 cm^{-1} decreased until it became stable confirming the presence of free isocyanate groups at the end of the arms. After adding the FAL in the second step, a gradual disappearance of NCO vibration band after 5 h of reaction was observed, while the intensities of absorptions bands of the urethane and the furan groups were emerged at 1530 cm^{-1} and 1422 cm^{-1}, respectively. Similar results were observed for the other PEG-F precursors.

The chemical structure of the expected PEG-F was verified by ^{1}H-NMR. All the PEG-F precursors show similar ^{1}H-NMR spectra. Herein, the ^{1}H-NMR spectrum of PEG-F_{60} was given as an example and depicted in Fig. 2. The presence of signals at 7.65 ppm (H_1), 7.56 ppm (H_{27}), 6.3 ppm ($H_{25,26}$), and 6.5 ppm ($H_{2,3}$) are assigned to the protons of the furanic nucleus, those at 3.5 ppm correspond to the protons ($H_{20,21}$) of PEG.

The average furan functionalities were verified by ^{1}H NMR spectrum. It was considered of 3, knowing that the ratio between the peaks H_1 and H_{27} relative to the furan group and the peak H_{16} of isocyanate was approximately close to the theoretical proportions.

DSC studies revealed that the designed PEG-F precursors are semi-crystalline polymers (Fig. S6 in SI). As shown by the data reported in Table 3, the melting point (Tm) was ranged from 21 to 36 °C, which is lower values than the initial PEG-diol (Tm = 47 °C). The melting enthalpy measured for PEG-F_{40} is very low (0.4 $J.g^{-1}$) compared to PEG-F_{60} and PEG-F_{90}, having a melting enthalpy of 64.0 and 72.0 $J.g^{-1}$, respectively. On the other hand, the glass transition of PEG-F_{40} is clearly defined, which is in agreement with its low rate of crystallinity.

It was found that both Tg and Tm values increase with increasing PEG and H_{12}MDI content in the formulation of furan-functionalized PEG. PEG-F_{60} and PEG-F_{90} own the highest Tm values compared to PEG-F_{40}. For example, PEG-F_{90} showed a Tm value of 36 °C, whereas PEG-F_{40} displayed a Tm of 21 °C. Concerning the glass transition, PEG-F_{90} showed the highest Tg value. Based on the molecular weights determined by SEC, PEG-F_{60} and PEG-F_{90} highlighted the shorter chain length molecules. So, this slight shift of Tg and Tm towards higher value may be explained by a greater density of rigid segments and hydrogen bonds due to isocyanate groups which reduce the movements of molecules and create more ordered phases [25, 26].

The molecular weights (number average molecular weight ($\overline{M_n}$), weight average molecular weights ($\overline{M_w}$), and polydispersity index (D_m) of the obtained PEG-F precursors are shown in Table 3. The results revealed that the number-average molecular weight of PEG-F_{40} was slightly higher than those of PEG-F_{60} and PEG-F_{90} which own close molecular weights (Fig. S7 in SI). Globally, molecular weight tends to decrease from PEG-F_{40} to PEG-F_{90} as

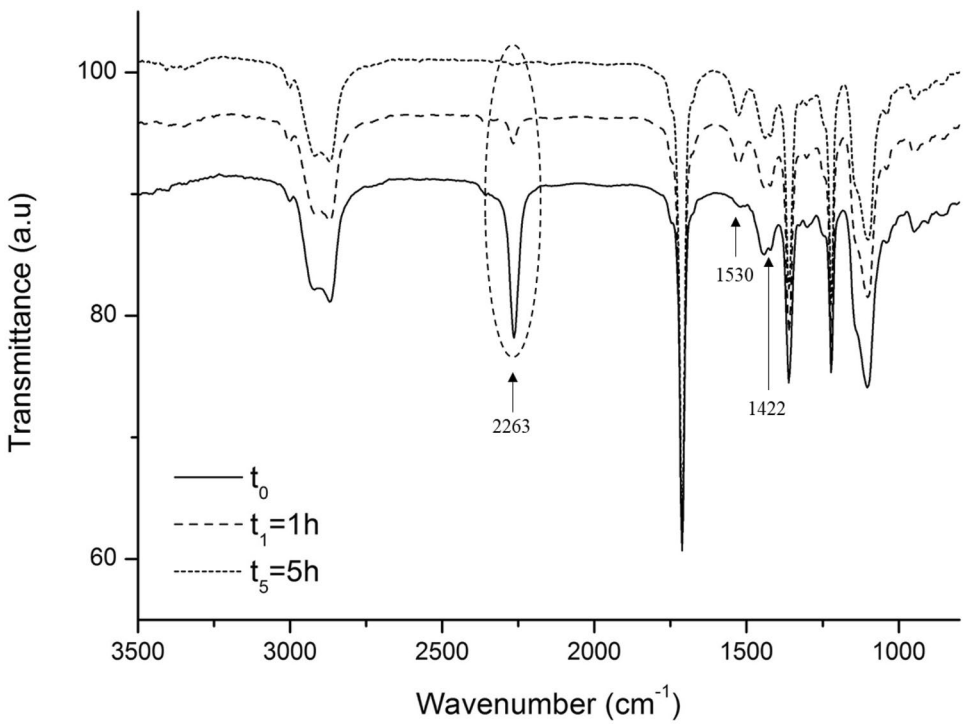

Fig. 1 FTIR spectra acquired at different reaction times from the reaction mixture of PEG-F_{60} synthesis

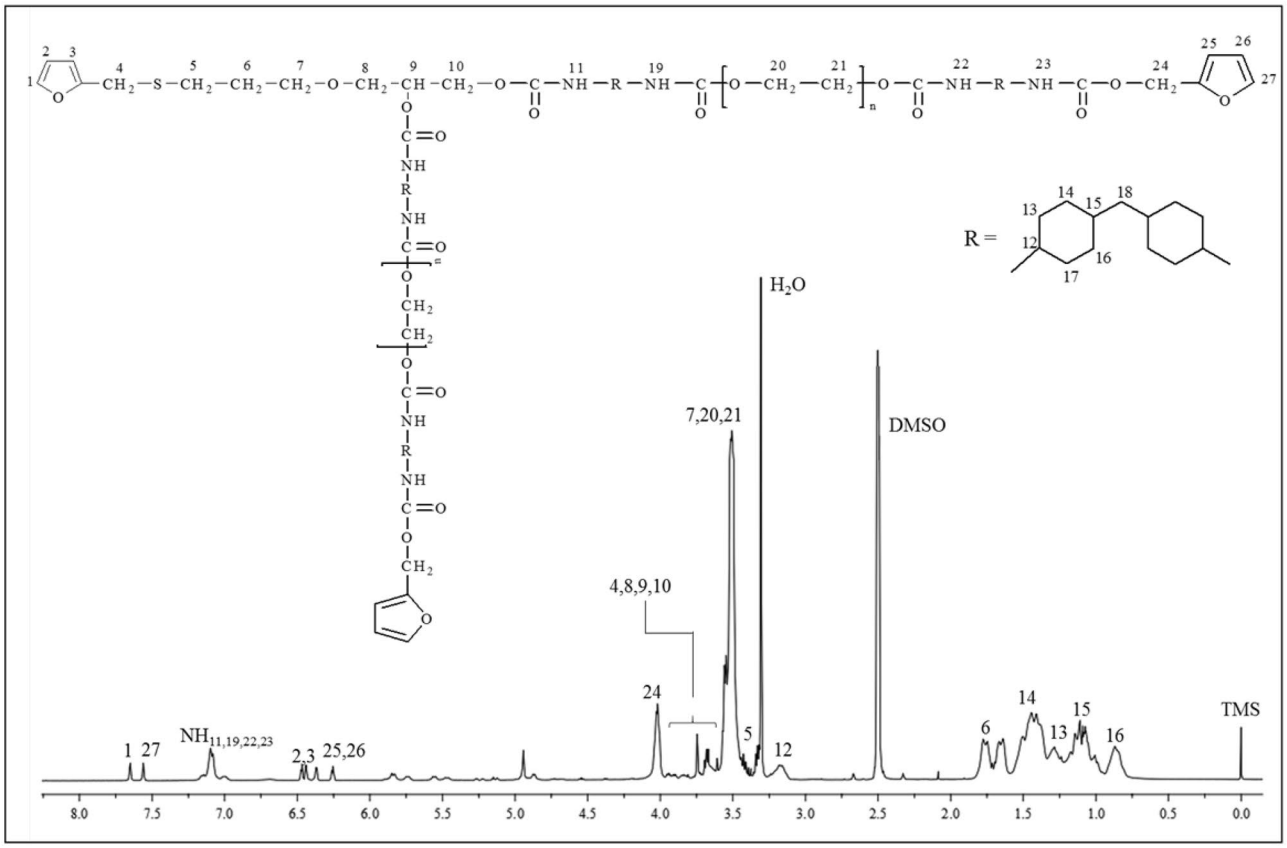

Fig. 2 ^{1}H-NMR spectrum of PEG-F_{60}

it has been observed by Gaina et al. [27] for the synthesis of cross-linked poly(ether-urethane)s. Authors noticed that by increasing the molar ratio of chain extender in the formulation isocyanate/polyol/chain extender, the average molecular weight of the polyurethane decreased. Dispersity index increases slightly from PEG-F_{40} to PEG-F_{90}, the last for which shorter chains are more present.

Synthesis of PLA-diol

Hydroxyl-telechelic PLA was obtained by ring opening polymerization of L-lactide using 1,4-butanediol as the co-initiator and stannous octoate as the catalyst (Scheme S1). The obtained PLA-diol had an average molecular weight of $\overline{M_n}$ = 780 g mol^{-1}, a $\overline{DP_n}$ of 10, and a Tg of − 12 °C.

The ^{1}H NMR characterization of PLA-diol was published in our previous work [23] and a typical ^{1}H NMR spectrum is given in Fig. S8 in SI.

Synthesis of maleimide-modified PLA (PLA-Tri M)

PLA-diol was grafted with maleimide groups in order to obtain the dienophile (PLA-Tri M) complementary to PEG-F with a maleimide functionality of 3. This synthesis was performed via the reaction between isocyanate and hydroxyl groups from previously prepared PLA-diol,

Table 3 Thermal properties and molecular weight data of PEG-F precursors

Samples	$\overline{M_n}^{a}$ (g. mol^{-1})	$\overline{M_w}$ (g.mol^{-1})	$\overline{M_n}^{a}$	Tg^{b} (°C)	Tm^{b} (°C)	$\triangle H_m{}^{b}$ (J. g^{-1})	Td$_{(5\%)}$ (°C)^{c}
PEG-F_{40}	6800	12,000	1.7	− 50	21	0.4	203
PEG-F_{60}	3600	6800	1.8	− 51	31	64.0	200
PEG-F_{90}	3500	6800	1.9	− 43	36	72.0	196

[a]Number average molecular weight, weight average molecular weight, and polydispersity index determined by SEC in THF

[b]Glass transition temperature, melting point, and melting enthalpy determined by DSC

[c]Degradation temperature at which a 5% weight loss was observed in TGA

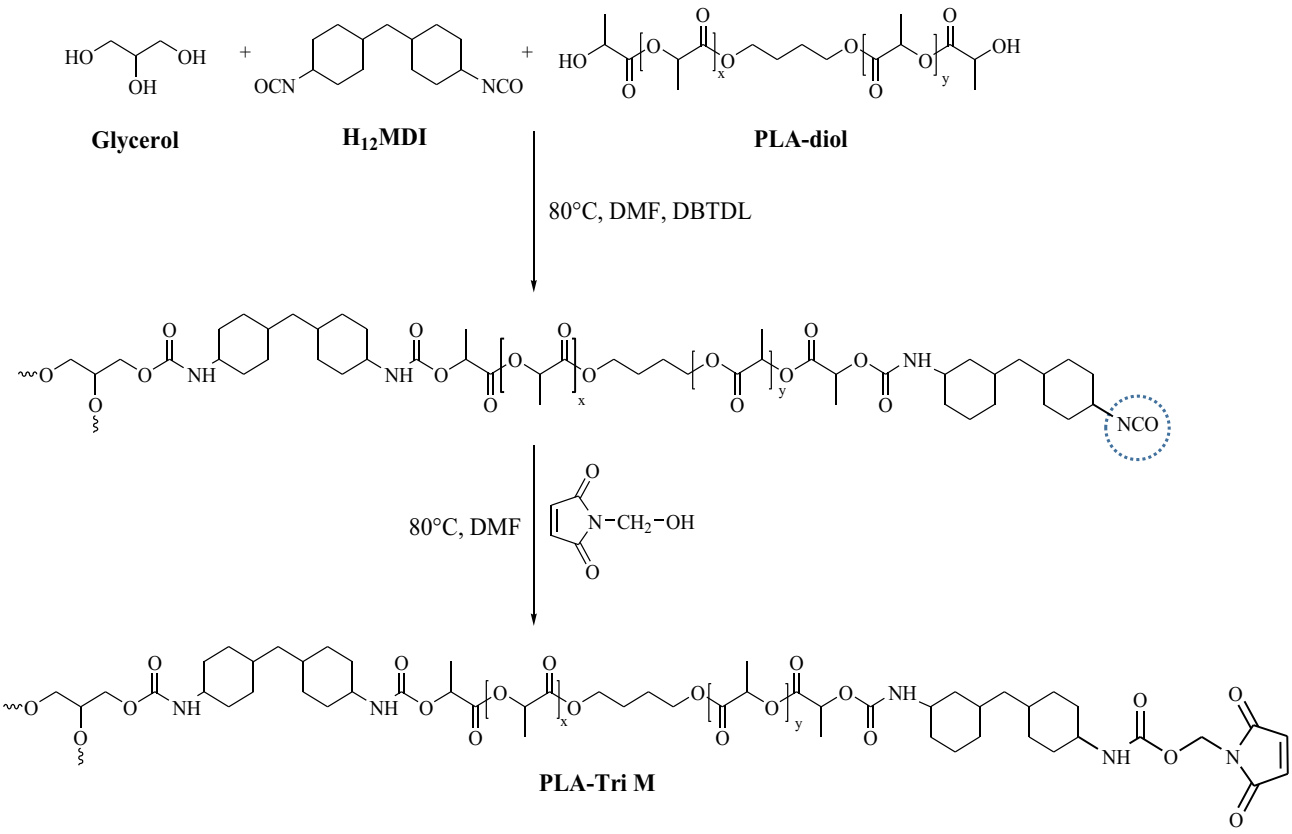

Scheme 3 Synthesis of PLA-Tri M

N-hydroxymethylmaleimide, diisocyanate (H_{12}MDI), and glycerol as a chain connector (Scheme 3). PLA-Tri M was characterized by FTIR, ^{1}H-NMR, and DSC.

To ascertain the grafting of maleimide functions to the PLA end arms, FTIR spectroscopy was used. Representative spectra of PLA-Tri M at different reaction times are given in Fig. S9 in SI.

In order to further confirm the chemical structure of PLA-Tri M, ^{1}H-NMR was performed and the spectrum is shown in Fig. 3. Signals at 1.4 and 5.2 ppm were assigned to the lactide unit protons, those at 7.3 ppm to the proton of the urethane function formed by the reaction between hydroxyl and isocyanate groups. We can notice the presence of peaks at 7.15 and 7.07 ppm which refer to the protons of maleimide confirming the success of maleimide grafting to PLA.

The number average molecular weight of PLA-Tri M was calculated from the ^{1}H-NMR spectrum according to the following equation as reported by Li et al. [28] with some modification:

$$\overline{M_n} = M_{(glycerol)} \times \alpha + M_{H12MDI} \times \beta + M_{PLA} \times \gamma + M_{HMM} \times \eta \quad (3)$$

where α, β, γ, and η are the molar numbers of glycerol, H_{12}MDI, PLA, and HMM reagent segments, respectively, whereas $M_{(glycerol)}$, $M_{(H12MDI)}$, $M_{(PLA)}$, and $M_{(HMM)}$ are their molar masses.

$$\frac{n_{H_{12}MDI}}{n_{glycerol}} = \frac{\beta}{\alpha} = \frac{\frac{I_8}{2}}{\frac{(I_1+I_2)}{5}} = \frac{5I_8}{2(I_1+I_2)} \quad (4)$$

The molar ratio of H_{12}MDI to glycerol can be calculated by the following equation using the integration of H_8, H_1, and H_2:

$$\frac{n_{HMM}}{n_{glycerol}} = \frac{\eta}{\alpha} = \frac{\frac{I_8}{2}}{\frac{(I_1+I_2)}{5}} = \frac{5I_{18}}{2(I_1+I_2)} \quad (5)$$

HMM/glycerol and PLA/glycerol molar ratios were obtained using the integration of H_{18}, H_{14}, H_1, and H_2:

$$\frac{n_{PLA}}{n_{glycerol}} = \frac{\gamma}{\alpha} = \frac{\frac{I_{14}}{4}}{\frac{(I_1+I_2)}{5}} = \frac{5I_{14}}{4(I_1+I_2)} \quad (6)$$

If α is normalized to 1, the $\overline{M_n}$ of PLA-Tri M can be calculated using Eq. (3).

The average functionality of maleimide was calculated from the ^{1}H NMR spectrum. The ratio between the peak

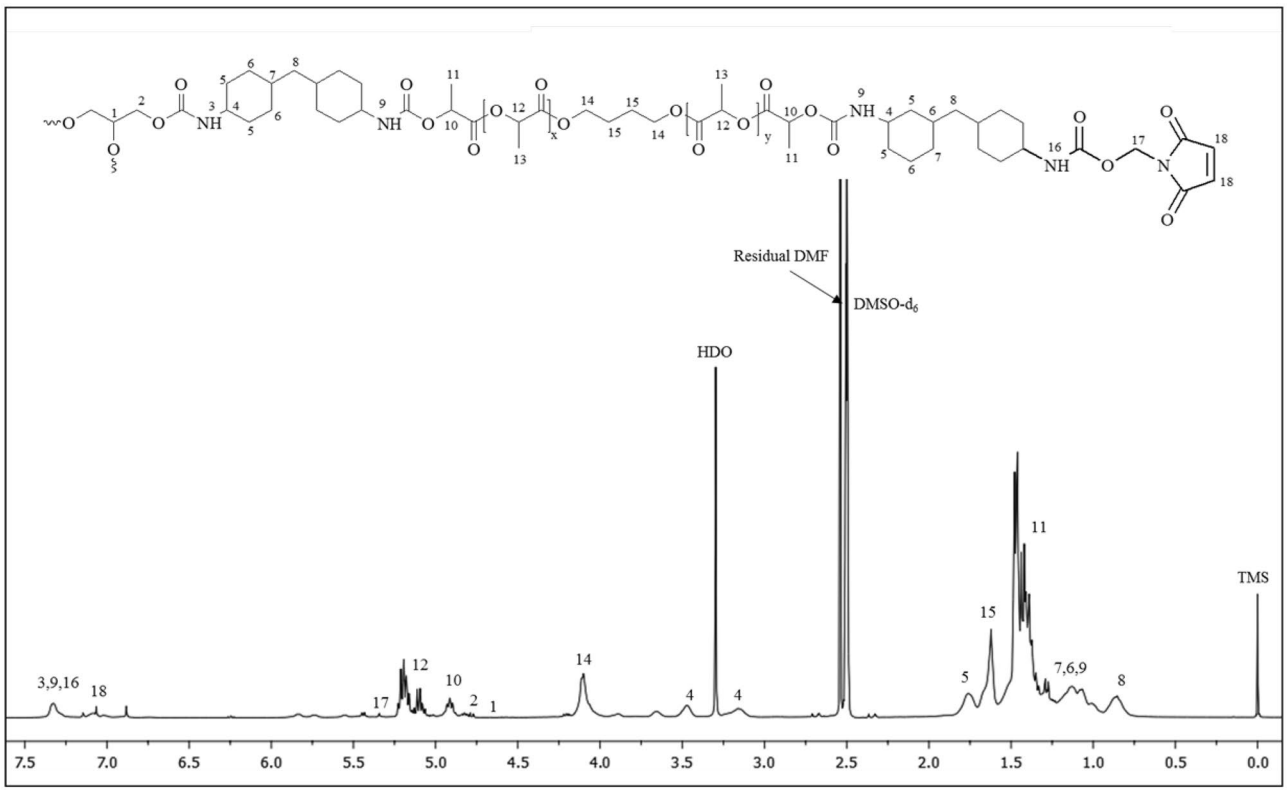

Fig. 3 ^{1}H-NMR spectrum of PLA-Tri M

at 7.07 ppm relative to the proton of maleimide (H_{18}) and the peak at 4.7 ppm relative to the proton of glycerol (H_2) gives a functionality of 2.7.

DSC analyses highlight the formation of an amorphous polymer with a glass transition temperature of 20 °C (Table 4).

Synthesis of adducts by Diels–Alder reaction and hydrogels

Before starting adducts' synthesis, both PEG-F and PLA-Tri M thermal stability were examined in order to ensure stable thermal behavior during extrusion. As an example, Fig. S10 in SI shows the comparison of PEG-F_{60} and PLA-Tri M TGA curves. Based on data obtained from thermogravimetric analysis (Tables 3 and 4 and Fig. S10), 90 °C was the selected mixing temperature as no weight loss was observed for both prepolymers at this temperature.

Thus, a series of hybrid adducts were prepared by mixing PLA-Tri M and PEG-F precursors in the extruder at 90 °C, followed by cooling to room temperature in order to achieve the network formation by DA reaction (Scheme S2 in SI). Hydrogels were further obtained from dried networks after immersion in water.

Theoretical node concentration (C_{node} in mol/cm^3) was calculated for each dry network using the following equation:

$$C_{node} = \frac{n_{multialcohol} \times \rho_{network}}{total\ mass} \quad (7)$$

Table 4 Thermal properties and molecular weight data of PLA-Tri M

Sample	$\overline{Mn}^a$ (g.mol^{-1})	$\overline{Mn}^b$ (g.mol^{-1})	$D_M{}^b$	Tg (°C)^c	$\bar{f}_{maleimide}$	$Td_{(5\%)}$ (°C)^d
PLA-Tri M	6500	7400	1.763	20	2.7	150

[a]Number average molecular weight determined by NMR in DMSO-d_6 at 80 °C.

[b]Number average molecular weight and polydispersity index determined by SEC in THF.

[c]Glass transition temperature taken as the inflection point of the DSC curves.

[d]Degradation temperature at which a 5% weight loss was observed in TGA.

where $n_{multialcohol}$ is the molar number of glycerol and furanic diol and $\rho_{network}$ is the density of networks.

Initial composition of networks was decided in order to have similar C_{node}. The obtained values of C_{node} are given in Table 7.

Networks and hydrogels characterization

FTIR network analysis

The occurrence of the Diels–Alder reaction in network synthesis was confirmed by FTIR. Figure 4 shows the spectra corresponding to the PEG-F_{60}, PLA-Tri M, and the final designed network $PE_{60}PL_{40}$. As it can be observed, the stretching vibration bands of the C = C bond at 1433 and 3093 cm^{-1} in furan and maleimide, respectively, were disappeared, whereas a new vibration band at 1652 cm^{-1} corresponding to C = C stretching in DA adduct appeared. The above results prove the total reaction between PEG-F and PLA-Tri M.

DSC network studies

The DSC curves of the various adducts during the first heating cycle are presented in Fig. S11 in SI. The results reveal the existence of two glass transition temperatures for each sample. The lowest Tg value is observed near − 20 °C, while a higher Tg value appears at around 50 °C. The existence of these two glass transitions which are distinctly different from those of the uncross-linked polymers (PEG-F and PLA-Tri M) proved the presence of two regions. On the other hand, there is no melting endotherm related to the presence of a crystalline phase as observed for PEG-F precursors, so the networks are completely amorphous. Interestingly, the first glass transition temperatures of the adducts are higher than the Tg of the uncross-linked PEG-F precursors and this might be due to the cross-linking of the chains reducing the free volume.

Regarding the second glass transition of the adducts, the values are all more important as the proportion of PEG-F precursors in the networks is high (Table 5). In view of the slight difference in theoretical node concentration between the networks, this gap in Tg values is attributed to the presence of more semi-crystalline PEG-F introduced in the formulation [29]. Notably, it can be seen from the DSC curves the presence of the large endothermic phenomenon corresponding to the rDA reaction of the thermosensitive networks centralized at 125 °C, with an enthalpy of 10 J/g.

Table 5 Tg values of Diels–Alder adducts

Designation	Tg_1 (°C)	Tg_2 (°C)	PEG-F content (%)
$PE_{40}PL_{60}$	− 18	42	40
$PE_{60}PL_{40}$	− 15	55	60
$PE_{90}PL_{10}$	− 11	57	90

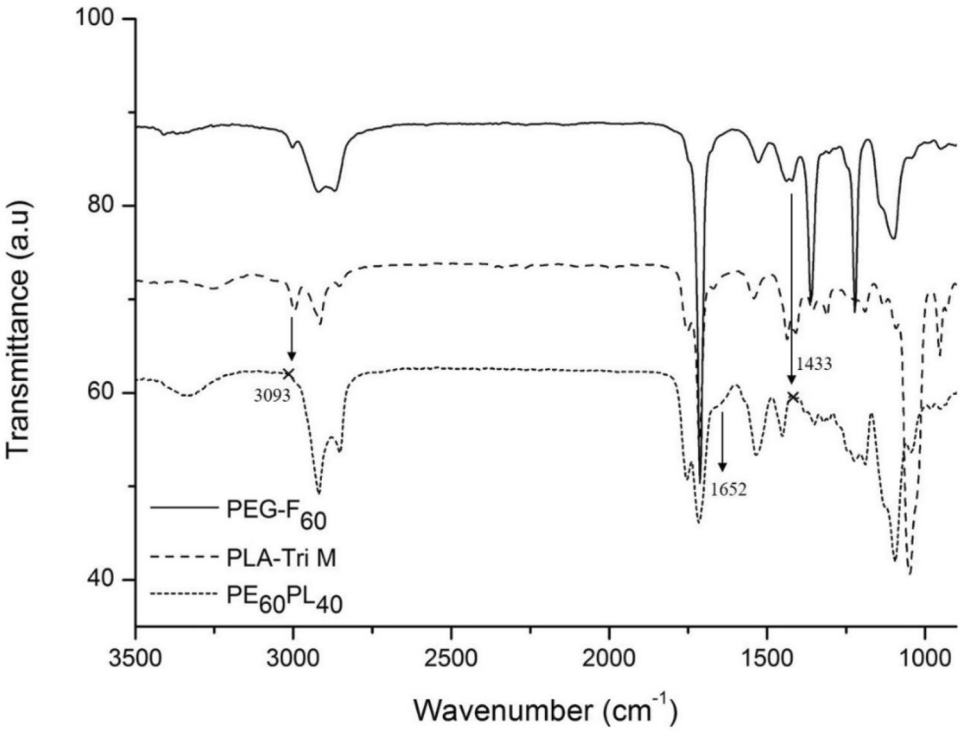

Fig. 4 FTIR spectra of PEG-F_{60}, PLA-Tri M, and the obtained network $PE_{60}PL_{40}$

These observations are in agreement with the studies of Avérous et al. [30].

Networks aqueous swelling studies

The swelling property of hydrogels is one of the most important criteria with regard to their use in biomedical applications. The presence of the hydrophilic PEG into the macromolecular network is expected to enhance the water uptake capacity of the hydrogel. Several parameters can affect the swelling behavior of hydrogels such as external conditions (temperature and pH), hydrogel structure, and cross-link concentration.

With the aim of studying the temperature sensitivity of our hydrogels, swelling studies were performed at two different temperatures: 25 °C and 37 °C. Figure 5 shows the equilibrium swelling values of all hydrogels' composition. As it can be seen, the swelling rates were higher at 37 °C than at 25 °C indicating that the swelling of hydrogels increases with temperature. This can be explained by the fact that when the temperature increases, the mobility of the polymer chains increases as well as the water diffusion, which makes the hydrogels swell easily [31].

The feed ratio of hydrophobic (PLA-Tri M) to hydrophilic (PEG-F) precursors influences the swelling rate of hybrid hydrogels. In fact, hydrogels absorb water until their weight reaches a plateau that represents the rate of swelling at equilibrium. This ratio is principally sensitive to the gels' composition and increases with the amount of hydrophilic PEG-F polymer. For example, at 25 °C, the 90:10 ratio of PEG-F/ PLA-Tri M shows a significantly high swelling rate, up to 73% at equilibrium compared with $PE_{60}PL_{40}$ which has a swelling rate of 56%, and with $PE_{40}PL_{60}$ which has the lowest swelling rate of 37%. These results are in agreement with the cross-linking density of the networks too. Indeed, an increase in the cross-link concentration leads to a decrease in the swelling behavior of the networks. In the case of this study, even if C_{node} values are similar, they differ slightly from each other (Table 7). For example, $PE_{40}PL_{60}$ owns the highest cross-linking node concentration $C_{node} = 0.139$ mmol cm^{-3}, and consequently has the lowest swelling rate.

In order to reveal the ability of hydrogels to be used as drug delivery system, Fick's model was used with a view to determine the water diffusion mechanism during the swelling process at 37 °C. For this, the diffusional coefficient n is calculated using the following equation for the first 60% of the fractional uptake:

$$F_t = M_t/M_i = K_1 t^n \tag{8}$$

where M_t and M_i represent the amount of water absorbed at time t and at equilibrium state, respectively, K_1 is a characteristic constant of the hydrogel, and n is the diffusional exponent of the solvent. The diffusional exponent n and K_1 are determined from the slope and intercept of the curves $\ln(M_t/M_i)$ as a function of ln (t).

For a water absorption fraction higher than 0.6, the Berens-Hopfenberg model [32] which takes into account the relaxation process is used (Eq. 9):

$$F_t = M_t/M_i = 1 - A.exp^{(-K_2 t)} \tag{9}$$

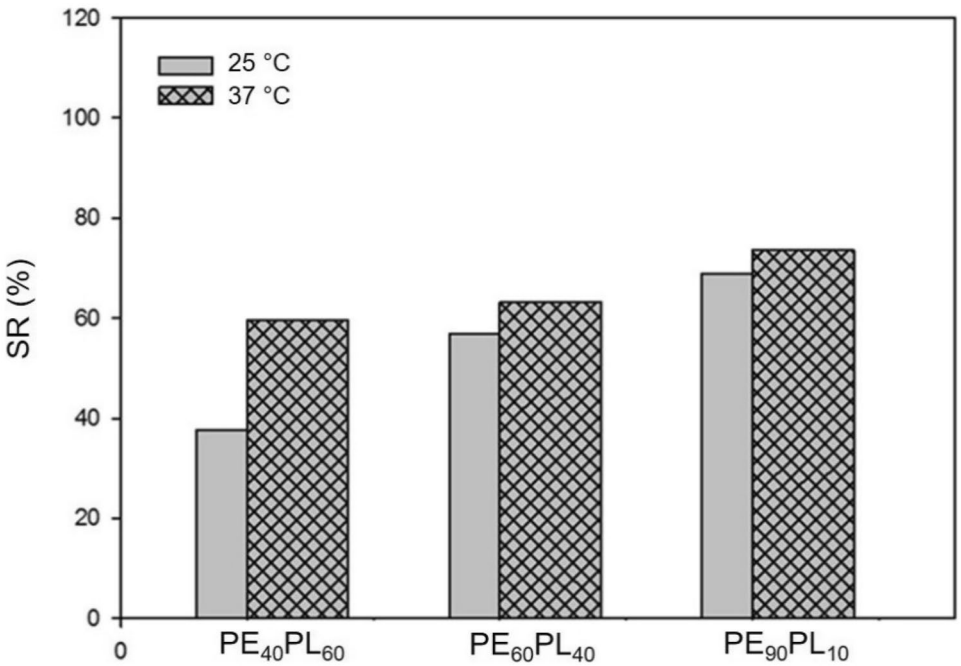

Fig. 5 Equilibrium swelling ratio of all hydrogels' composition at 25 °C and 37 °C in H_2O

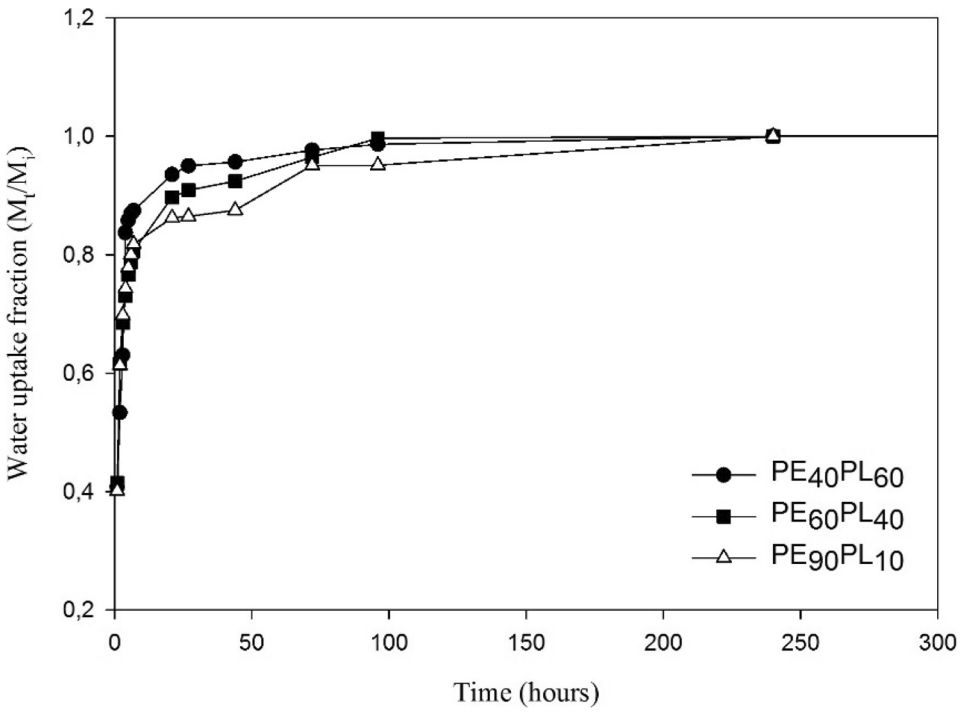

Fig. 6 Water uptake fraction of the various hydrogel compositions as a function of time in water at 37 °C

where M_t and M_i represent the amount of water absorbed at time t and at equilibrium state, respectively and K_2 and pre-exponential factor A are constants and are calculated from the slope and intercept of the plots of $\ln(1-M_t/M_i)$ as a function of t.

The normalized experimental curves representing the water absorption fraction over time $(M_t/M_i) = f(t)$ are shown in Fig. 6. For each curve, a first increase in the water absorption until reaching a first plateau is observed, and then followed by another increase of water uptake to finally reach a second plateau corresponding to the maximum absorption rate. This behavior is more pronounced for the $PE_{90}PL_{10}$ adduct, showing that water diffusion occurs in several stages and is affected by the content of hydrophilic polymer.

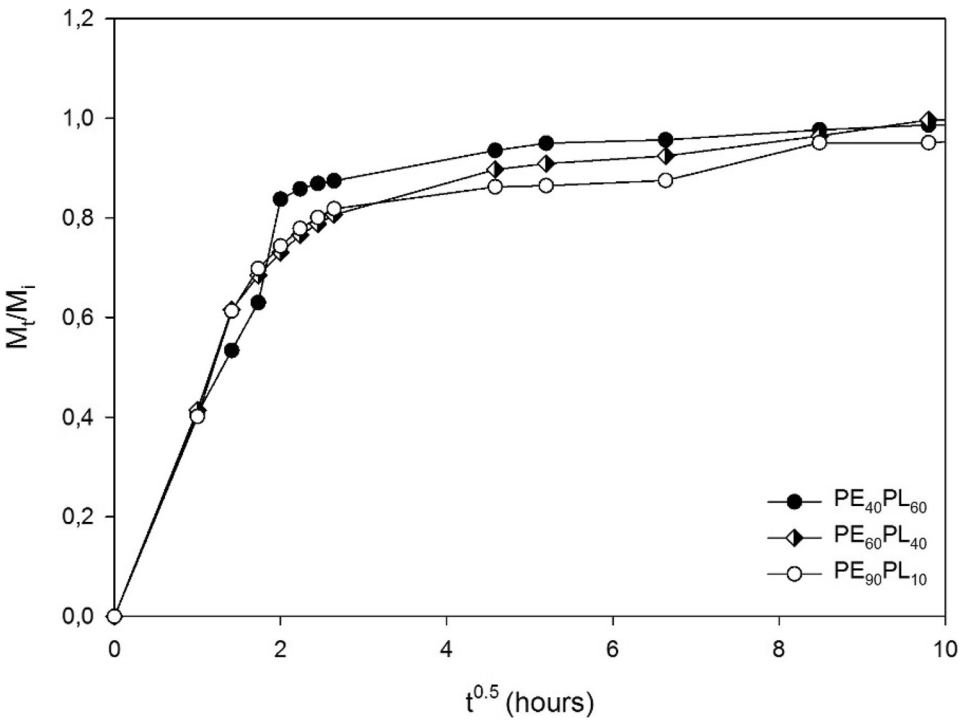

Fig. 7 Water uptake fraction of the various hydrogel compositions as a function of $t^{0.5}$

Table 6 Kinetic parameters of water absorption in adducts 37 °C

Samples	n	$K_1(h^{-n})$	A	$K_2(h^{-1})$
$PE_{40}PL_{60}$	0.387	0.408	0.153	0.020
$PE_{60}PL_{40}$	0.468	0.422	0.303	0.047
$PE_{90}PL_{10}$	0.610	0.401	0.485	0.148

Table 7 Thermo-mechanical properties of Diels–Alder adducts

Samples	G' (Pa)	C_{node} (mmol cm^{-3})	$T_{crossover}$ (°C) Min–Max
$PE_{40}PL_{60}$	6247	0.139	107–110
$PE_{60}PL_{40}$	9363	0.135	105–114
$PE_{90}PL_{10}$	31,031	0.113	97–110

First, to check for a Fickian behavior, $(M_t/M_i) = f(t^{0.5})$ curves were plotted (Fig. 7). Curves show that the M_t/M_i ratio seems to be proportional to $t^{0.5}$ for the very first initial part of the curves. Indeed, curves are linear on the 60% of the fractional uptake for PE_{60}/PLA_{40} and only on the 40% of the fractional uptake for the other adducts, suggesting a more evidenced Fickian behavior for PE_{40}/PLA_{60}.

Then, swelling diffusional exponents n, K_1, and K_2 of the hybrid hydrogels were calculated from Eqs. 8 and 9 and listed in Table 6. Obtained fitted curves are given in Fig. S12 in SI.

The values of the diffusional coefficient n and the constant K_1, calculated from the slope of the curves ln (Mt /Mi) as a function of ln(t) for M_t/M_i less than 0.6, are given in Table 6. The values of the constants K_1 do not seem to be affected by the composition of the adducts, knowing that the theoretical node concentrations are close from one adduct to another. On the other hand, it is noted that the value of n increases with the proportion of PEG in the network. The value of n is used for determining the diffusion type [33]. Indeed, n values less than 0.5 are attributed to a pseudo-Fickian behavior and n value of 0.5 to a Fickian behavior, while n values comprised between 0.5 and 1 is the reflection of anomalous diffusion type and for n values higher than 1, to a super case diffusion type [34]. The diffusional coefficient for $PE_{40}PL_{60}$ and $PE_{60}PL_{40}$ networks is 0.387 and 0.468, respectively; it can be said that water diffusion in these adducts follows a pseudo-Fickian behavior, whereas n is equal to 0.610 for $PE_{90}PL_{10}$ adduct, which indicates an anomalous type diffusion.

Finally, the Berens-Hopfenberg model is applied for M_t/M_i greater than 0.6. The results show that the greater the amount of hydrophilic polymer is, the greater the chain relaxation seems to control the water absorption. Indeed, the value of K_2 increases with the proportion of PEG in the networks.

Rheological characterization

Dynamic rheological analysis was investigated in order to study the viscoelastic properties of the designed materials before swelling, i.e., for dry Diels–Alder adducts and after swelling in water (hydrogels). Diels–Alder adducts were subjected to temperature sweep experiments to check the thermosensitive properties and especially the heat-reversibility of these adducts via the DA and rDA reactions.

- Frequency sweep test at 80 °C for Diels–Alder adducts

Frequency sweep tests were performed at 80 °C after a maturation period to ensure thermodynamic equilibrium. As seen in Fig. 8a, this test revealed that storage modulus (G') values of all adducts were constant in the low frequency region and significantly higher than those found for G″ indicating the typical solid-like gels characteristics [35].

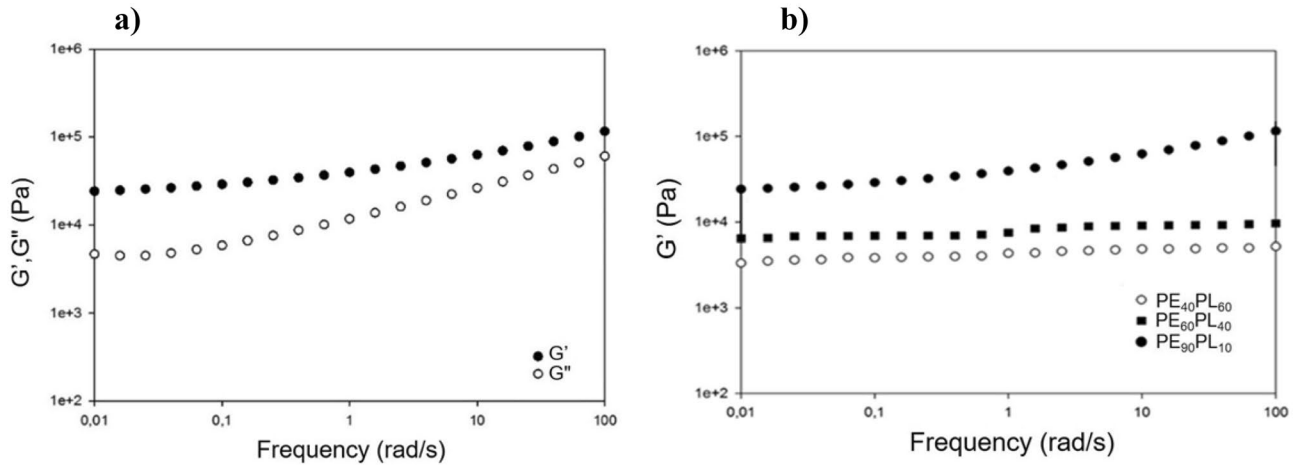

Fig. 8 Frequency sweep measurement at 80 °C of **a** $PE_{90}PL_{10}$ and **b** all adduct compositions

The values of G' at 1 rad.s^{-1} of DA adducts are reported in Table 7. By comparing the G' curves obtained for all networks, it is obvious that the presence of PEG block in the structure of the hybrid network improves the elasticity properties. As one can see on Fig. 8b, the $PE_{90}PL_{10}$ curve is well above the two other curves and its shape is slightly different. This behavior could suggest a better pressure-sensitive adhesive property for this formulation. From these results, it can be confirmed that the thermomechanical properties of the hydrogels depend on the PLA/PEG level in the network structure. Similar observations have been reported by Martinez et al. [36] who observed a decrease in G' and G″ values as the PLA content increase in the hydrogel structure.

- Temperature sweep tests for Diels–Alder adducts

In order to verify the reversible character of the obtained adducts, temperature sweep experiments were carried out at a constant frequency of 1 rad.s^{-1}. Fig. S13 in SI (a, b, c, and d) shows the results obtained with $PE_{90}PL_{10}$. The experiments were started at a high temperature to be above the de-cross-linking temperature. After cooling, the sample was then subjected to a maturation test at 80 °C for a few hours to promote the DA reaction until equilibrium. Two heating/cooling cycles were conducted from 80 to 130 °C and 130 to 80 °C, respectively. Fig. S13 (a, b) and Fig. S13 (c, d) show the results obtained during the first cycle (cooling and heating) and the second cycle (cooling and heating), respectively. They highlight the crossing of the G' and G″ curves as a function of temperature. The crossover point, named $T_{crossover}$, indicates a nominal transition from elastic behavior to viscous state. Below the $T_{crossover}$, the reaction of Diels–Alder is predominant compared to the reaction of retro Diels–Alder. During heating, the number of network connections decreases and the equilibrium is more and more driven from the DA adduct to the formation of the reagents. The network is then destroyed, as it is seen with solubility tests in DMSO at high temperature. This trend has been already confirmed for xylan-based networks obtained via Diels–Alder reaction [37–39].

Values of $T_{crossover}$ are given in Table 7. They are all around 110 °C with slightly lower values for $PE_{90}PL_{10}$, probably due to its lower C_{node} value.

The thermoreversibility of the Diels–Alder networks was further confirmed by the solubility tests. In fact, at 25 °C, the networks were not soluble in DMSO, which is a good solvent of both PEG-F and PLA-Tri M precursors, whereas at high temperature of 130 °C, all the networks were almost dissolved in DMSO. These results confirm the reversible character of DA networks.

- Frequency sweep tests for hydrogels

Hydrogels were also subjected to rheological tests. First, all samples were submitted to a strain sweep test to establish the linear viscoelastic region where G' and G″ are independent of the applied strain. Frequency sweep tests were then performed at 25 °C and 37 °C for the different hydrogel compositions. A typical frequency sweep test of $PE_{90}PL_{10}$ adduct at 37 °C and 25 °C is shown in Fig. 9.

As it can be observed, G' is weakly dependent of the frequency and always greater than G″ confirming the solid-like structure and the elastic behavior of the samples. However, it is important to notice that G' and G″ are almost parallel on the frequency range suggesting a fractal gel rheological behavior in this frequency range [40]. Additional

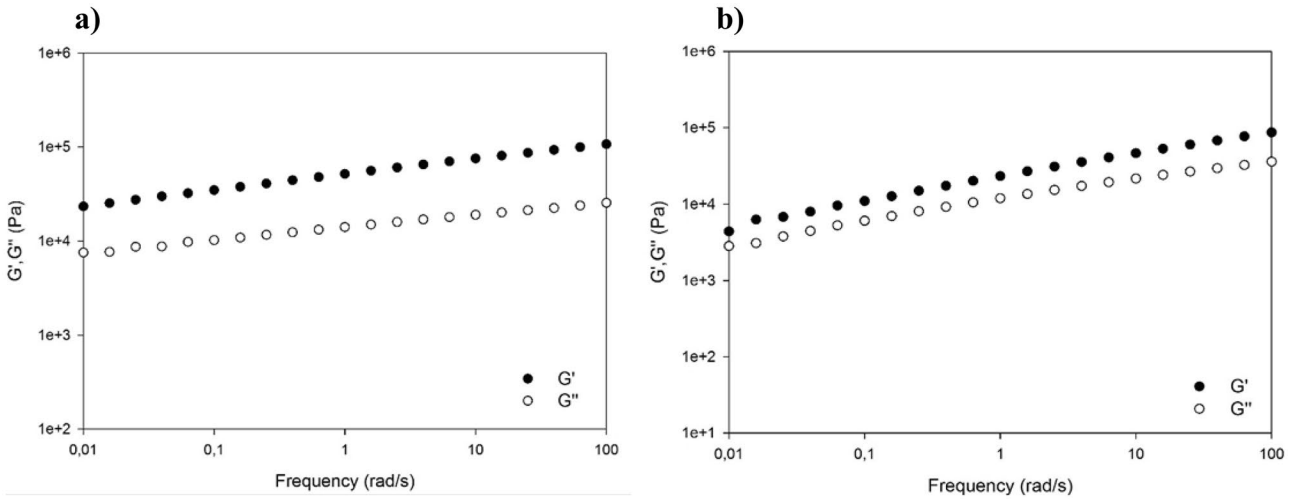

Fig. 9 Frequency sweep of $PE_{90}PL_{10}$ after swelling at **a** 25 °C, **b** 37 °C

measurements at lower frequency would have resulted in a lower and more correct G' value but there is a risk to a water loss with long-time analysis.

Comparing the rheological behavior of $PE_{90}PL_{10}$ before (Fig. 8a) and after swelling in water (Fig. 9b), it can be observed that there is a gradual decrease of G' and G″ with the frequency at 37 °C. In fact, during swelling, the intermolecular distance increases with temperature and the water occupies the space between the cross-linking nodes leading to a decrease in G' value.

Whereas, Fig. 9a shows almost the same behavior that obtained with the dry adduct (Fig. 8a) and this could correspond to a little swelled hydrogel for which the water occupies only the free volume.

The consistent tendency of G' proved the success and suitability of the DA cross-linking reaction for hydrogel formation.

Using biodegradable polymers for hydrogels preparation is a selected criterion to the field of biomedical applications as scaffolds or implants. The rheological characterization of hydrogels is therefore of great relevance of the final material as it could be directly affecting its final performance. As indicator of the rigidity, G' values of the obtained hydrogels were found to be in the range between 10^3 and 10^4 Pa, which are comparable with those values of nerve tissue [41].

Degradation

It has been clearly established in the literature that degradation is an important feature for the development of biomaterials. Understanding the degradation mechanisms of polymers in the body is important for designing a particular controlled release system. In order to examine the

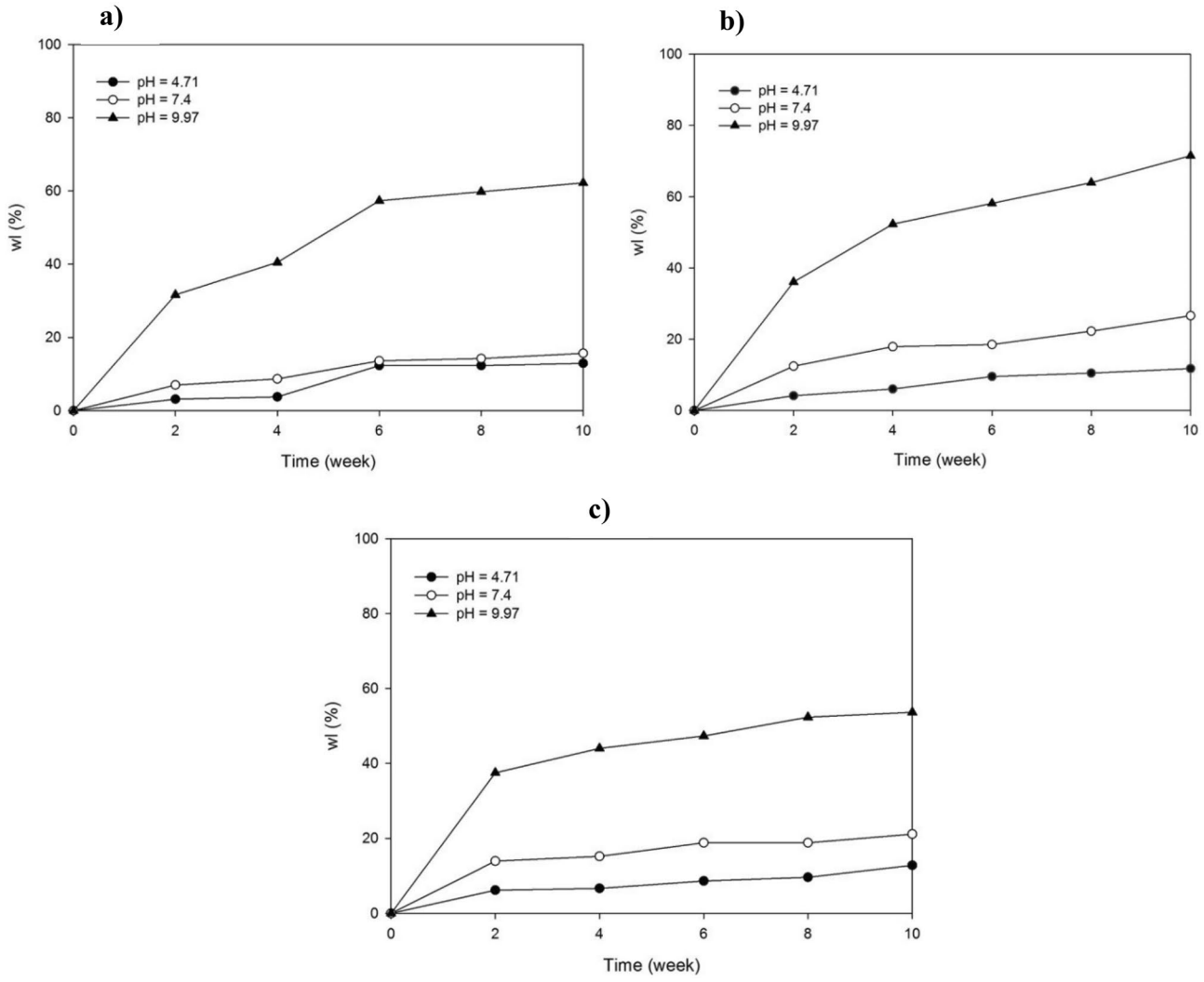

Fig. 10 Hydrolytic degradation of the various hydrogel compositions in different pH values at 37 °C: **a** $PE_{40}PL_{60}$, **b** $PE_{60}PL_{40}$, **c** $PE_{90}PL_{10}$

degradability of prepared hydrogels, hydrolytic degradation was evaluated.

Hydrolytic degradation

It is obvious that the degradation of hydrogels in solution depends on several parameters such as cross-linking density and molecular weight [42]. In another aspect, the hydrophilicity of the macromolecular structure also plays a very important role in the rate of degradation of the hydrogels.

In order to simulate human body conditions, the hydrolytic degradation of hydrogels was investigated in three different media (pH = 4.71, 7.4 and 9.97) at 37 °C over a period of 10 weeks. Figure 10 shows the evolution of the weight loss percentage of hydrogels as function of degradation time. As depicted, the immersion of hydrogels in different pH leads to their hydrolytic degradation with quite different kinetics, which was strongly dependent on their composition and their properties.

The first observation with regard to these curves is that there are two distinct steps during the hydrolysis of hydrogels. From the beginning until the second week, the hydrolytic degradation begins rapidly. Then, from the 2nd week until the end, a second stage of degradation occurs until a maximum degradation rate is reached.

We can also notice that alkaline hydrolysis resulted in a higher weight loss than either acidic or neutral hydrolysis. This weight loss reached after 10 weeks 65% and 70%, in basic medium, in the case of $PE_{40}PL_{60}$ and $PE_{60}PL_{40}$, respectively. One possible reason for this is that degradation at a higher pH is expected to be enhanced due to the presence of a high concentration of hydroxy (OH^-) ions that can catalyze cleavage of the PLA-Tri M ester bonds [43]. Moreover, hydroxy ions can induce the ring-opening hydrolysis of maleimide groups [44]. Indeed, it has been revealed that DA hydrogels swell at pH = 5.5 but dissolve after 4 days in a basic medium. So, the more the content of PLA-Tri M in the network is, the higher the reached % weight loss is. Under acidic conditions, weight loss percentage reaches only 10% after 10 weeks. It could be due to a partial neutralization of the acidic medium functions by the urethane functions, which protects the ester bond to hydrolytic degradation [45]. At pH = 7.4, the hydrolytic degradation of networks is low and the % weight loss is only about 20% after 10 weeks of adducts immersion. For the first weeks of immersion, the greater the PEG-F content is, the more rapid the degradation is. This is in agreement with the experimental water diffusion curves $M_t/M_i = f(t)$ (Fig. 6).

It is not at all excluded too that polyester urethane functions, because of their great affinity for water molecules to which they can associate by hydrogen bonding, cause the hydrophilicity of the macromolecular chains to be accentuated, thus favoring their contact with water and consequently their degradation by hydrolysis [46].

Conclusions

A series of hybrid hydrogels based on PEG and PLA were successfully synthesized through Diels–Alder reaction. This approach was adopted to provide a green synthesis without the participation of any additives or catalysts. By varying the furan-containing hydrophilic PEG and PLA-modified maleimide ratio, different compositions of DA adduct were obtained via extrusion process at 90 °C. Once synthesized, the gels were swelled with water to form the hydrogels. The success of the DA reaction in the formation of a thermoreversible cross-linked structure was confirmed by rheological studies. Swelling analysis revealed the temperature sensitivity of the hydrogels and the influence of the content of hydrophilic polymer in water diffusion mechanism.

Finally, hydrolytic degradation studies confirmed that an increase in hydrophilic polymer PEG-F leads to an increase of water diffusion into the networks' structure and therefore an increase in the degradation rate due to the presence of hydrolytically sensitive ester groups.

Supplementary Information The online version contains supplementary material available at https://doi.org/10.1007/s10965-022-03153-9.

Acknowledgements The authors acknowledge the NMR Polymer Center of the Institut de Chimie de Lyon for assistance.

Funding This work was financially supported by the Ministry of foreign affairs and international development in France for Eiffel Scholarship, Rhône Alpes for CMIRA scholarship and the Ministry of Higher Education, Scientific Research and Technology in Tunisia.

Declarations

Conflict of interest The authors declare no competing interests.

References

1. Chang H, Li C, Huang R, Su R, Qi W, He Z (2019) Amphiphilic hydrogels for biomedical applications. J Mater Chem B 7:2899–2910. https://doi.org/10.1039/C9TB00073A
2. Gao Y, Deng A, Wu X, Sun C, Qi C (2021) Injectable multiresponsive hydrogels cross-linked by responsive macromolecular micelles. React Funct Polym 161:104866. https://doi.org/10.1016/j.reactfunctpolym
3. Farhat W, Venditti R, Mignard N, Taha M, Becquart F, Ayoub A (2017) Polysaccharides and lignin based hydrogels with potential pharmaceutical use as a drug delivery system produced by a reactive extrusion process. Int J Biol Macromol 104:564–575. https://doi.org/10.1016/j.ijbiomac.2017.06.037
4. Ullah F, Othman MBH, Javed F, Ahmad Z, Akil HM (2015) Classification, processing and application of hydrogels: a

review. Mater Sci Eng: C Mater Biol Appl 57:414–433. https://doi.org/10.1016/j.msec.2015.07.053
5. Ali A, Ahmed S (2018) Recent advances in edible polymer based hydrogels as a sustainable alternative to conventional polymers. J Agric Food Chem 66:6940–6967. https://doi.org/10.1021/acs.jafc.8b01052
6. Madduma-Bandarage USK, Madihally SV (2020) Synthetic hydrogels: synthesis, novel trends, and applications. J Appl Polym Sci 138:50376. https://doi.org/10.1002/app.50376
7. Francisco AT, Hwang PY, Jeong CG, Jing L, Chen J, Setton LA (2014) Photocrosslinkable laminin-functionalized polyethylene glycol hydrogel for intervertebral disc regeneration. Acta Biomater 10:1102–1111. https://doi.org/10.1016/j.actbio.2013.11.013
8. Nguyen MK, Alsberg E (2014) Bioactive factor delivery strategies from engineered polymer hydrogels for therapeutic medicine. Prog Polym Sci 39:1235–1265. https://doi.org/10.1016/j.progpolymsci.2013.12.001
9. Bakaic E, Smeets NMB, Hoare T (2015) Injectable hydrogels based on poly(ethylene glycol) and derivatives as functional biomaterials. RSC Adv 5:35469–35486. https://doi.org/10.1039/C4RA13581D
10. Vashist A, Vashist A, Gupta YK, Ahmad S (2014) Recent advances in hydrogel based drug delivery systems for the human body. J Mater Chem B 2:147–166. https://doi.org/10.1039/C3TB21016B
11. James R, Manoukian OS, Kumbar SG (2016) Poly(lactic acid) for delivery of bioactive macromolecules. Adv Drug Deliv Rev 107:277–288. https://doi.org/10.1016/j.addr.2016.06.009
12. Li L, Cao ZQ, Bao RY, Xie BH, Yang MB, Yang W (2017) Poly(L-lactic acid)-polyethylene glycol-poly(L-lactic acid) triblock copolymer: a novel macromolecular plasticizer to enhance the crystallization of poly(L-lactic acid). Eur Polym J 97:272–281. https://doi.org/10.1016/j.eurpolymj.2017.10.025
13. Metters AT, Anseth KS, Bowman CN (2000) Fundamental studies of a novel, biodegradable PEG-b-PLA hydrogel. Polymer 41:3993–4004. https://doi.org/10.1016/S0032-3861(99)00629-1
14. Mondal S, Das S, Nandi AK (2020) A review on recent advances in polymer and peptide hydrogels. Soft Matter 16:1404–1454. https://doi.org/10.1039/C9SM02127B
15. Buwalda SJ, Vermonden T, Hennink WE (2017) Hydrogels for therapeutic delivery: current developments and future directions. Biomacromol 18:316–330. https://doi.org/10.1021/acs.biomac.6b01604
16. Yu F, Cao X, Li Y, Zeng L, Yuan B, Chen X (2014) An injectable hyaluronic acid/PEG hydrogel for cartilage tissue engineering formed by integrating enzymatic crosslinking and Diels-Alder "click chemistry." Polym Chem 5:1082–1090. https://doi.org/10.1039/C3PY00869J
17. Guaresti O, Garcia-Astrain C, Palomares T, Alonso-Varona A, Eceiza A, Gabilondo N (2017) Synthesis and characterization of a biocompatible chitosan- based hydrogel cross-linked via 'click' chemistry for controlled drug release. Int J Biolog Macromo 102:1–9. https://doi.org/10.1016/j.ijbiomac.2017.04.003
18. Gregoritza M, Brandl FP (2015) The Diels-Alder reaction: a powerful tool for the design of drug delivery systems and biomaterials. Eur J Pharm Biopharm Part B 97:438–453. https://doi.org/10.1016/j.ejpb.2015.06.007
19. Gandini A (2013) The furan/maleimide Diels-Alder reaction: a versatile click-unclick tool in macromolecular synthesis. Prog Polym Sci 38:1–29. https://doi.org/10.1016/j.progpolymsci.2012.04.002
20. Gheneim R, Perez-Berumen C, Gandini A (2002) Diels-Alder reactions with novel polymeric dienes and dienophiles: synthesis of reversibly cross-linked elastomers. Macromolecules 35:7246–7253. https://doi.org/10.1021/ma020343c
21. Gandini A, Carvalho AJF, Trovatti E, Kramer RK, Lacerda TM (2018) Macromolecular materials based on the application of the Diels-Alder reaction to natural polymers and plant oils. Eur J Lipid Sci Technol 120:1700091. https://doi.org/10.1002/ejlt.201700091
22. Tawney P, Synder R, Conger R, Leibbrand K, Stiteler C, Williams A (1961) The chemistry of maleimide and its derivatives. II. Maleimide and N-methylolmaleimide J Org Chem 26:15–21. https://doi.org/10.1021/jo01060a004
23. Djidi D, Mignard N, Taha M (2015) Thermosensitive polylactic-acid-based networks. Ind Crop. Prod 72:220–230. https://doi.org/10.1016/j.indcrop.2014.09.035
24. Mhiri S, Mignard N, Abid M, Prochazka F, Majeste JC, Taha M (2017) Thermally reversible and biodegradable polyglycolic-acid-based networks. Eur Polym J 88:292–310. https://doi.org/10.1016/j.eurpolymj.2017.01.020
25. Panwiriyarat W, Tanrattanakul V, Chueangchayaphan N (2017) Study on physicochemical properties of poly(ester-urethane) derived from biodegradable poly(ε-caprolactone) and poly(butylene succinate) as soft segments. Polym Bull 74:2245–2261. https://doi.org/10.1007/s00289-016-1833-x
26. Seidler K, Ehrmann K, Steinbauer P, Rohatschek A, Andriotis OG, Dworak C, Koch T, Bergmeister H, Grasl C, Schima H, Thurner PJ, Liska R, Baudis S (2018) A structural reconsideration: linear aliphatic or alicyclic hard segments for biodegradable thermoplastic polyurethanes? J Polym Sci Part A: Polym Chem 56:2214–2224. https://doi.org/10.1002/pola.29190
27. Gaina C, Ursache O, Gaina V, Varganici CD (2013) Thermally reversible cross-linked poly(ether-urethane)s. eXPRESS Polym Lett 7:636–650. https://doi.org/10.3144/expresspolymlett.2013.60
28. Li X, Becquart F, Taha M, Majeste JC, Chen J, Zhang S, Mignard N (2020) Tuning the thermoreversible temperature domain of PTMC-based networks with thermosensitive links concentration. Soft Matter 16:2815–2828. https://doi.org/10.1039/C9SM01882D
29. Zhang C (2006) Elastic degradable polyurethane for biomedical applications. ProQuest.
30. Duval A, Couture G, Caillol S, Avérous L (2017) Biobased and aromatic reversible thermoset networks from condensed tannins via the Diels-Alder reaction. ACS sustainable Chem Eng 5:1199–1207. https://doi.org/10.1021/acssuschemeng.6b02596
31. Gupta NV, Shivakumar HG (2012) Investigation of swelling behavior and mechanical properties of a pH-sensitive superporous hydrogel composite. Iran J Pharm Res 11:481–493. https://doi.org/10.22037/IJPR.2012.1097
32. Kim B, Kristen LF, Peppas NA (2003) Dynamic swelling behavior of pH-sensitive anionic hydrogels used for protein delivery. J Appl Polym Sci 89:1606–1613. https://doi.org/10.1002/app.12337
33. Neogi P (1996) Diffusion in Polymer. Marcel Dekker, New York., pp 147–171
34. Panpinit S, Pongsomboon SA, Keawin T, Saengsuwan S (2020) Development of multicomponent interpenetrating polymer network (IPN) hydrogel films based on 2-hydroxyl methacrylate (HEMA), acrylamide (AM), polyvinyl alcohol (PVA) and chitosan (CS) with enhanced mechanical strengths, water swelling and antibacterial properties. React Funct Polym 156:104739. https://doi.org/10.1016/j.reactfunctpolym.2020.104739
35. Almdal K, Dyre J, Hvidt S, Kramer O (1993) Towards a phenomenological definition of the term 'gel.' Polym Gels Networks 1:5–7. https://doi.org/10.1016/0966-7822(93)90020-I
36. Martinez VS, Olalde B, Redondo DM, Braceras I, Morin F, Valero J, Castro B (2014) Degradable poly(ethylene glycol)-based hydrogels: synthesis, physico-chemical properties and in vitro characterization. J Bioactive Compatible Polym 29:270–283. https://doi.org/10.1177/0883911514528597

37. Farhat W, Venditti RA, Becquart F, Ayoub A, Majesté JC, Taha M, Mignard N (2019) Synthesis and characterization of thermoresponsive xylan networks by Diels-Alder reaction. ACS App Polym Mater 1:856–866. https://doi.org/10.1021/acsapm.9b00095
38. Strachota B, Morand A, Dybal J, Matějka L (2019) Control of Gelation and properties of reversible Diels-Alder networks: design of a self-healing network. Polymers 11:930. https://doi.org/10.3390/polym11060930
39. Chapelle C, Quienne B, Bonneaud C, David G, Caillol S (2020) Diels-Alder-Chitosan based dissociative covalent adaptable networks. carbohydr Polym 253:117222. https://doi.org/10.1016/j.carbpol.2020.117222
40. Winter HH (1987) Evolution of rheology during chemical gelation. Prog Colloid Polym Sci 75:104–110. https://doi.org/10.1007/BFb0109413
41. Matricardi P, Meo CD, Coviello T, Hennink WE, Alhaique F (2013) Interpenetrating polymer networks polysaccharide hydrogels for drug delivery and tissue engineering. Adv Drug Deliv Rev 65:1172–1187. https://doi.org/10.1016/j.addr.2013.04.002
42. Kharkar PM, Kiick KL, Kloxin AM (2013) Designing degradable hydrogels for orthogonal control of cell microenvironments. Chem Soc Rev 42:7335–7372. https://doi.org/10.1039/C3CS60040H
43. Tsuji H, Ikarashi K (2004) In vitro hydrolysis of poly(L-lactide) crystalline residues as extended-chain crystallites: III. Effects of pH and enzyme. Polym Degrad Stab 85:647–656. https://doi.org/10.1016/j.polymdegradstab.2004.03.004
44. Kirchhof S, Strasser A, Wittmann HJ, Messmann V, Hammer N, Goepferich AM, Brandl FP (2015) New insights into the crosslinking and degradation mechanism of Diels-Alder hydrogels. J Mater Chem B 3:449–457. https://doi.org/10.1039/C4TB01680G
45. He X, Zhang X, He J, Liu F (2018) Preparation and properties of hydroxyl-terminated cationic waterborne polyurethanes for cathodic electrodeposition coating. Adv Polym Technol 37:3831–3841. https://doi.org/10.1002/adv.22166
46. Opera S (2012) Degradation of crosslinked poly(ester-urethanes) elastomers in distilled water: influence of hard segment. J Appl Polym Sci 124:1059–1066. https://doi.org/10.1002/app.35196